Magnetic properties of paramelaconite (Cu_4O_3): A pyrochlore lattice with $S=\frac{1}{2}$

L. Pinsard-Gaudart,[1] J. Rodríguez-Carvajal,[2] A. Gukasov,[2] and P. Monod[3]
[1]*Laboratoire de Physico-Chimie de l'Etat Solide, Orsay, France*
[2]*Laboratoire Léon Brillouin (CEA-CNRS), CEA/Saclay, France*
[3]*Laboratoire de Physique des Solides, ESPCI, Paris, France*
(Received 30 July 2003; revised manuscript received 26 September 2003; published 16 March 2004)

We have studied the magnetic properties of a single crystal of the mineral paramelaconite, Cu_4O_3, showing a tetragonally distorted (space group $I4_1/amd$) magnetic pyrochlore sublattice of $S=1/2$. The magnetic susceptibility shows a drop around 40 K that could be interpreted as an antiferromagnetic transition or the appearance of a nonmagnetic state at lower temperatures. Neutron diffraction measurements at low temperature show unambiguously the transition to an ordered state of propagation vector $\mathbf{k}=(1/2,1/2,1/2)$ with respect to the reciprocal basis of the conventional body centered cell. Referred to the pseudocubic $Fd3m$ setting it is $\mathbf{k}_C=(0,1,1/2)$. To the best of our knowledge, this is an unprecedented magnetic ordering in pyrochlore lattices. We argue that the observed magnetic ordering cannot be explained within models limited to isotropic superexchange interactions.

DOI: 10.1103/PhysRevB.69.104408 PACS number(s): 75.25.+z, 75.10.Pq, 61.12.Ld

INTRODUCTION

The appearance or absence of magnetic order in topologically frustrated lattices is a subject of current strong interest.[1,2] Magnetic frustration comes from the fact that there is no spin configuration that simultaneously minimizes all the pair energies of the whole set of bonds in the structure. The simplest case is the equilateral triangle with identical magnetic atoms in the vertices connected by negative [antiferromagnetic (AF)] exchange interactions. The most common and simple lattices based on triangular units are the hexagonal (triangular) and *kagome* lattices in two dimensions (2D) and the fcc and pyrochlore lattices in 3D. The nature of the ground state in these systems is still of controversial nature, especially for the quantum mechanical case $S=1/2$. For classical spins interacting via isotropic exchange, triangle and tetrahedral clusters adopt a ground state with zero total spin. In extended lattices there is an infinite number of configurations satisfying the local zero spin state for each triangle/tetrahedron. This gives rise to an infinitely degenerated ground state. In some circumstances, quantum or thermal fluctuations are able to select a particular ground state configuration and magnetic order can be observed (*order by disorder* concept introduced by Villain[3]). In real materials the presence of longer-range exchange interactions and anisotropy may provide other ways for breaking the degeneracy and establish a complex (noncollinear and/or incommensurate) long-range magnetic order [e.g., FeF_3 (Ref. 4)]. In some cases spin-glass behavior have been observed (e.g., $Y_2Mo_2O_7$) and in others (especially for quasi 2D *kagome* case) no ordering is detected, the experiments suggesting a spin liquid behavior (e.g., SCGO, some jarosites) see Refs. 1, 2.

The materials having a pyrochlore magnetic lattice are quite common but most of them concern rare earth or transition metals having large spins. It is expected that quantum effects are maximized for $S=1/2$, so the search for Cu^{+2} pyrochlore (and in general frustrated) lattices is important to understand the nature of the magnetic ground state in these lattices.

Paramelaconite Cu_4O_3 is a rare copper oxide intermediate between CuO and Cu_2O; its crystal structure, of symmetry $I4_1/amd$ (see Fig. 1), was determined by O'Keeffe and J. Bovin.[5] It was described as a compound formed by chains of square CuO_4 units sharing edges, as in $CuGeO_3$, that cross perpendicularly as shown schematically in Fig. 1. This suggests that paramelaconite may be also an AF 1D $S=1/2$ compounds. A close analysis of the Cu^{2+} sublattice shows that it forms a slightly distorted pyrochlore arrangement. This makes paramelaconite, as far as we know, the first $S=1/2$ pyrochlore lattice that is being studied experimentally from the magnetic point of view.

EXPERIMENTAL

We have studied a single crystal of Cu_4O_3 ($5\,mm^3$) provided by the Smithsonian Institute (Washington DC) of mineral origin.[6] Up to date, attempts to prepare this compound in bulk form, free from parasitic phases have been unsuccessful. However, thin films obtained by sputtering under controlled conditions have recently provided synthetic paramelaconite in pure form.[7] Indeed extraction of copper or its oxides with concentrated aqueous ammonia was found to produce a mixture of CuO, Cu_2O.[8] Magnetic susceptibility measurements were performed in a superconducting quantum interference device (SQUID) magnetometer for two preoriented settings of the crystal.

Neutron diffraction studies were carried out at the Orphée reactor (LLB), in Saclay. Integrated intensities were measured on the four-circle diffractometer 6T2 in a Displex refrigerator using neutrons of wavelengths 1.5 and 0.9 Å. Crystal and magnetic structure refinements were based on the measured squares of structure factors using the program FULLPROF.[9]

RESULTS

Magnetic susceptibility. The compound is an insulator and its magnetic susceptibility shows a transition around 40 K.

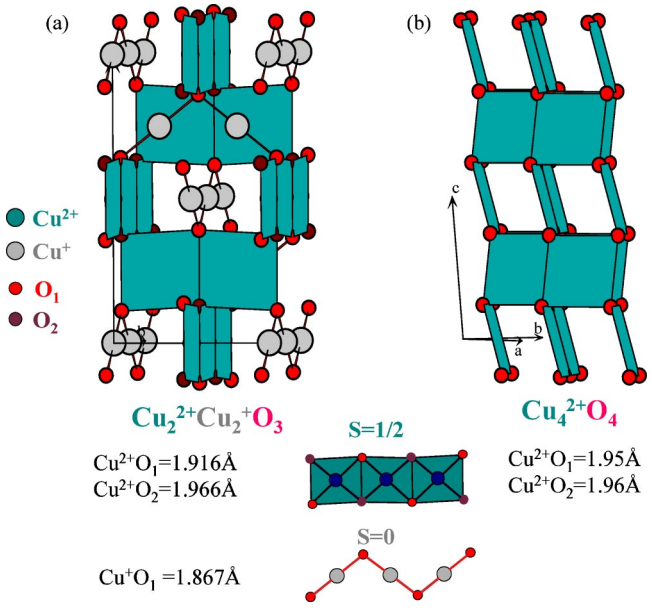

FIG. 1. (Color online) (a) Crystal structure of paramelaconite Cu_4O_3. (b) Crystal structure of tenorite CuO for comparison.

The presence of magnetic impurities manifests itself by a Curie law tail at low temperature (estimated to correspond to $\approx 10^{-3}$) and by a hump near 230 K, which is tentatively attributed to the presence of 5% of CuO. However, the shape of the susceptibility curve suggests either an AF ordering or the presence of a nonmagnetic ground state (spin liquid) at low temperature. We observe a Curie-Weiss behavior ($\theta_W \approx 900$ K) at high temperature down to a round maximum at 75K followed by a transition at 42.3(1) K marked by a discontinuity of the slope that is anisotropic (see Fig. 2). Above 42 K the 10% anisotropy of the susceptibility ($\chi_a > \chi_c$) can easily be attributed to a g factor anisotropy although no ESR of Cu^{2+} has been detected on this compound.[10] Below 42 K χ_c remains approximately constant but χ_a drops linearly by about a factor 2. The strength of the applied magnetic field does not change the transition temperature within 1K between 0.5 and 5 T.

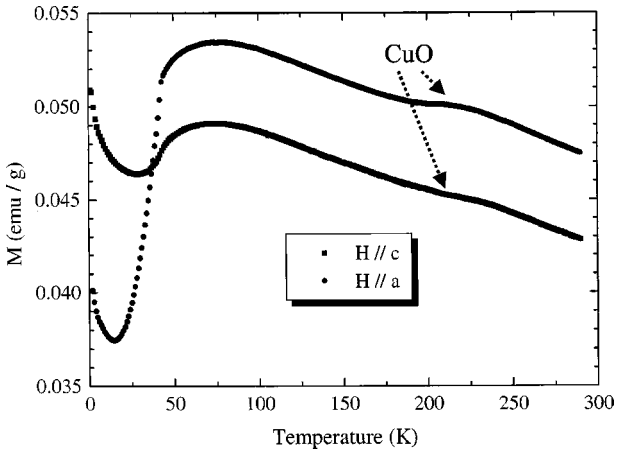

FIG. 2. Magnetization of a single crystal of Cu_4O_3 measured under a field of 1 T for $H \| a$ and $H \| c$. The hump near 230 K is attributed to traces of CuO.

Crystal structure. The crystal structure of paramelaconite was established by O'Keeffe *et al.*[5] We used the structural parameters for starting refinements of the data measured at RT and 7 K. The final refined structure parameters are not significantly different from those obtained at room temperature by O'Keeffe. The structure consists of alternating chains of edge-sharing square planar CuO_4 and zigzag chains of linear coordinated copper ions. These chains runs parallel to **a** and **b** consecutively on moving along **c**. $Cu_2Ag_2O_3$ (Ref. 11) is isostructural and isoelectronic with Cu_4O_3. The magnetic susceptibility of $Cu_2Ag_2O_3$ (Refs. 12, 13) shows the same behavior as the Cu_4O_3, which again suggests either an antiferromagnetic phase transition or the transition to a nonmagnetic ground state. A neutron diffraction study on $Cu_2Ag_2O_3$ has shown the presence of a structural phase transition at the same temperature as the drop in susceptibility takes place.[14] In the case of paramelaconite we have not observed a splitting of the Bragg peaks below 40 K, but the results of our refinements indicate an increase of the thermal displacement parameters that may hide a similar phase transition that we are not able, within our resolution conditions, to resolve. In Tables I and II we give a summary of the results obtained for the refinement of the crystal and magnetic structures.

A comparison of the structures of tenorite (CuO) and paramelaconite shows that the Cu-O atomic arrangements are similar in the two cases. The monoclinic unit cell of tenorite has the following dimensions: $a = 4.6837$ Å, $b = 3.4226$ Å, $c = 5.1288$ Å, and $\beta = 99.54°$.[15] The unit cell contains four chemical units of CuO and its space group is $C2/c$. Each Cu atom is surrounded by four O atoms in a planar arrangement at the corners of a rectangle (distances Cu-O: 1.95 and 1.96 Å). Four Cu atoms at the corners of a nonequilateral tetrahedron surround each O atom.

In the paramelaconite structure the addition of oxygen atoms at sites corresponding to the *4a* positions (0, 3/4, 1/8) converts a rod of Cu^{+} into a rod of Cu^{2+} together with the new rod of oxygen atoms. Figure 1 shows how the mutually perpendicular paths of CuO_4 groups in the oxygen-inserted paramelaconite are shared to produce the CuO structure. The main difference is that the four equal Cu-O bonds in tenorite are respectively elongated and shortened by pairs in paramelaconite. From the point of view of the magnetic properties, the difference between these two compounds is considerable. The absence of the additional Cu^{2+} rod in paramelaconite changes totally the topology of the magnetic lattice. The suppression of the set of exchange interactions concerned with this row in CuO, gives rise to the same magnetic topology.

Magnetic structure. A low-temperature single crystal neutron diffraction experiment in 6T2 has shown clearly the appearance of very weak magnetic reflections below 41 K that can be indexed using the propagation vector $\mathbf{k} = (1/2,1/2,1/2)$. From the dependence of the magnetic reflection (1/2 1/2 3/2), shown in Fig. 3, the Néel temperature was evaluated to be $T_N = 41$ K in good agreement with the transition observed by susceptibility measurements. The analysis of intensity of this magnetic reflection as a function of temperature gives a critical exponent $\beta = 0.230(3)$ significantly

TABLE I. Results of the crystal structure refinement of Cu_4O_3 ($T=7$ K).

Atom		x	y	z	B (Å^2)
Cu(1)	*8c*	0	0	0	1.80(10)
Cu(2)	*8d*	0	0	1/2	1.89(10)
O(1)	*8e*	0	1/4	0.1162(2)	2.11(11)
O(2)	*4b*	0	1/4	3/8	1.98(12)
$a=b=5.822$ Å, $c=9.844$ Å					
Space group			$I4_1/amd$		
Number of variables			21		
wavelength			0.9 Å	1.5 Å	
max sin Θ/λ			0.63 Å^{-1}	0.40 Å^{-1}	
Nuclear reflections N_{obs}			73	32	
R factor (F^2)			6.50%	5.26%	
χ^2			6.2	6.9	

lower than that expected for a 3D Heisenberg system ($\beta=0.367$), indicating low dimensional or frustrated behavior.

Since the magnetic reflections are rather weak (inset of Fig. 3) there is no unique solution for the spin configuration. A symmetry analysis of the propagation vector group[16] gives rise to basis functions of the irreducible representations that do not constraint strongly the possible solutions. In the Appendix, we present a summary of our symmetry analysis, performed with the help of the program BASIREPS.[17] We have assumed a simple subset of symmetry constraints for refining the magnetic structure of Cu_4O_3. Our discussion here will be limited to the two more plausible solutions: collinear (pseudosinusoidal, model 1) and noncollinear (helical-like, model 2) configurations. The propagation vector $\mathbf{k}=(1/2,1/2,1/2)$ is at the surface of the Brillouin zone of the space group $I4_1/amd$, but $\mathbf{k}$ is not equivalent to $-\mathbf{k}$ so that the possible magnetic structures are described by the two arms of the star, $\mathbf{k}$ and $-\mathbf{k}$. The magnetic moments in the crystal are calculated through the following Fourier series:

$$\mathbf{m}_{lj}=\sum_{\mathbf{k}}\mathbf{S}_{\mathbf{k}j}\exp(-2\pi i\mathbf{k}\cdot\mathbf{R}_l)=\mathbf{S}_{\mathbf{k}j}\exp(-2\pi i\mathbf{k}\cdot\mathbf{R}_l)+\mathbf{S}_{-\mathbf{k}j}\exp(2\pi i\mathbf{k}\cdot\mathbf{R}_l),$$

where the index j runs from 1 to 4 atoms per primitive cell and l is a composite index for a lattice translation. In our frame, lattice vectors are of the form $\mathbf{R}_l=l_1\mathbf{a}+l_2\mathbf{b}+l_3\mathbf{c}$, where l_i are all integers or half-integers (centering translation). The four Cu ions, constituting the content of a primitive cell, have as components, referred to the conventional I-centered cell Cu(2)-1: (0,0,1/2); Cu(2)-2: (1/4,3/4,3/4); Cu(2)-3:(1/2,0,0); and Cu(2)-4: (1/4,1/4,1/4).

To get real magnetic moments the relation $\mathbf{S}_{-\mathbf{k}j}=\mathbf{S}^*_{\mathbf{k}j}$ must be obeyed. The Fourier coefficients may be generally written as

$$\mathbf{S}_{\mathbf{k}j}=\frac{1}{2}(\mathbf{S}^R_{\mathbf{k}j}+i\mathbf{S}^I_{\mathbf{k}j})\exp(-2\pi i\phi_j)$$

so that

TABLE II. Results of the magnetic structure refinements of Cu_4O_3 ($T=7$ K). Phases are given in fractions of 2π.

Atoms	x	y	z	Phase ϕ_j (sinusoidal)	Phase ϕ_j (helical)	Phase ϕ_j (group theory)
Cu(2)-1	0	0	1/2	0	0	0
Cu(2)-2	1/4	3/4	3/4	−0.010(15)	0.005(11)	0
Cu(2)-3	1/2	0	0	0.243(12)	0.263(8)	0.25
Cu(2)-4	1/4	1/4	1/4	−0.245(14)	−0.261(9)	−0.25
Wavelength		0.9 Å		1.5 Å		
max sin Θ/λ		0.63 Å^{-1}		0.40 Å^{-1}		
Magnetic reflections N_{obs}		89		32		
		Model 1	Model 2	Model 1	Model 2	
Magnetic R-factor ($\lvert\mathbf{F}_\perp\rvert$)		26.7%	16.8%	16.6%	15.7%	
χ^2		5.6	2.2	6.0	4.4	
			Model 1	Model 2		
m (μB)Cu^{2+}			0.66(2)	0.46(2)		

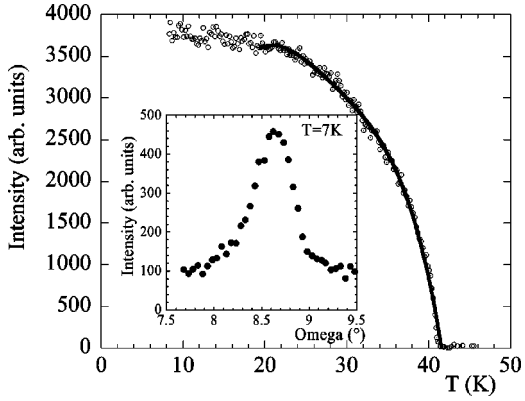

FIG. 3. Intensity of the magnetic reflection (1/2, 1/2, 3/2) as a function of temperature. The inset corresponds to the omega scan around the (1/2, 1/2, 3/2) magnetic peak position.

$$\mathbf{m}_{lj} = \mathbf{S}^R_{\mathbf{k}j} \cos 2\pi(\mathbf{k}\cdot\mathbf{R}_l + \phi_j) + \mathbf{S}^I_{\mathbf{k}j} \sin 2\pi(\mathbf{k}\cdot\mathbf{R}_l + \phi_j).$$

Depending on the relations between vectors $\mathbf{S}^R_{\mathbf{k}j}$ and $\mathbf{S}^I_{\mathbf{k}j}$, the above equation corresponds to a quite general set of four interpenetrated complex helices. If the imaginary component is zero, the structure corresponds to a set of four interpenetrated sinusoids.

We may further simplify our description if we assume the same amplitude and the same unit vectors along the real (**u**) and imaginary (**v**) components for all atoms (uniaxial sinusoid and single axis helix). The value of the phase ϕ_j determines the relative orientation of the different magnetic moments of atoms in cell of origin $\mathbf{R}_l$. The lattice vectors $\mathbf{R}_l$ have components l_i that may be all integer or half-integers when using the conventional crystallographic frame (I-centered cell).

The most simple spin arrangements that give reasonable agreement with the experimental data can be described as follows.

(1) Uniaxial sinusoidal:

$$\mathbf{S}^R_{\mathbf{k}j} = \mu^s_{\mathrm{Cu}}\mathbf{u}, \quad \mathbf{S}^I_{\mathbf{k}j} = 0,$$

$$\mathbf{m}_{lj} = \mu^s_{\mathrm{Cu}} \cos 2\pi(\mathbf{k}\cdot\mathbf{R}_l + \phi_j)\mathbf{u},$$

$$\mathbf{m}_j(l_1, l_2, l_3) = \mu^s_{\mathrm{Cu}} \cos \pi(l_1 + l_2 + l_3 + 2\phi_j)\mathbf{u}.$$

(2) Single axis helix:

$$\mathbf{S}^R_{\mathbf{k}j} = \mu^h_{\mathrm{Cu}}\mathbf{u}, \quad \mathbf{S}^I_{\mathbf{k}j} = \mu^h_{\mathrm{Cu}}\mathbf{v}, \quad \mathbf{u}\cdot\mathbf{v} = 0,$$

$$\mathbf{m}_{lj} = \mu^h_{\mathrm{Cu}} \cos 2\pi(\mathbf{k}\cdot\mathbf{R}_l + \phi_j)\mathbf{u} + \mu^h_{\mathrm{Cu}} \sin 2\pi(\mathbf{k}\cdot\mathbf{R}_l + \phi_j)\mathbf{v},$$

$$\mathbf{m}_j(l_1, l_2, l_3) = \mu^h_{\mathrm{Cu}} \cos \pi(l_1 + l_2 + l_3 + 2\phi_j)\mathbf{u} + \mu^h_{\mathrm{Cu}} \sin \pi(l_1 + l_2 + l_3 + 2\phi_j)\mathbf{v}.$$

In the particular case of the observed propagation vector, we have $\mathbf{k} = 1/4\mathbf{H}$, where **H** is a reciprocal lattice vector of the nuclear structure. For such a case the sinusoidal structures are constant moment structures by assuming an additional appropriate global phase that does not change the calculated diffraction pattern.

For these kind of magnetic structures group theory fixes the value of the phases (see the Appendix) but we have also considered them as free parameters, so that we have refined the amplitude μ^s_{Cu} or μ^h_{Cu}, and the three phases ϕ_2, ϕ_3, and ϕ_4. The phase of the first atom is arbitrarily fixed to zero. The unit vectors **u** and **v** have been taken along **a** and **b**, respectively, this means that the helical model has the unique

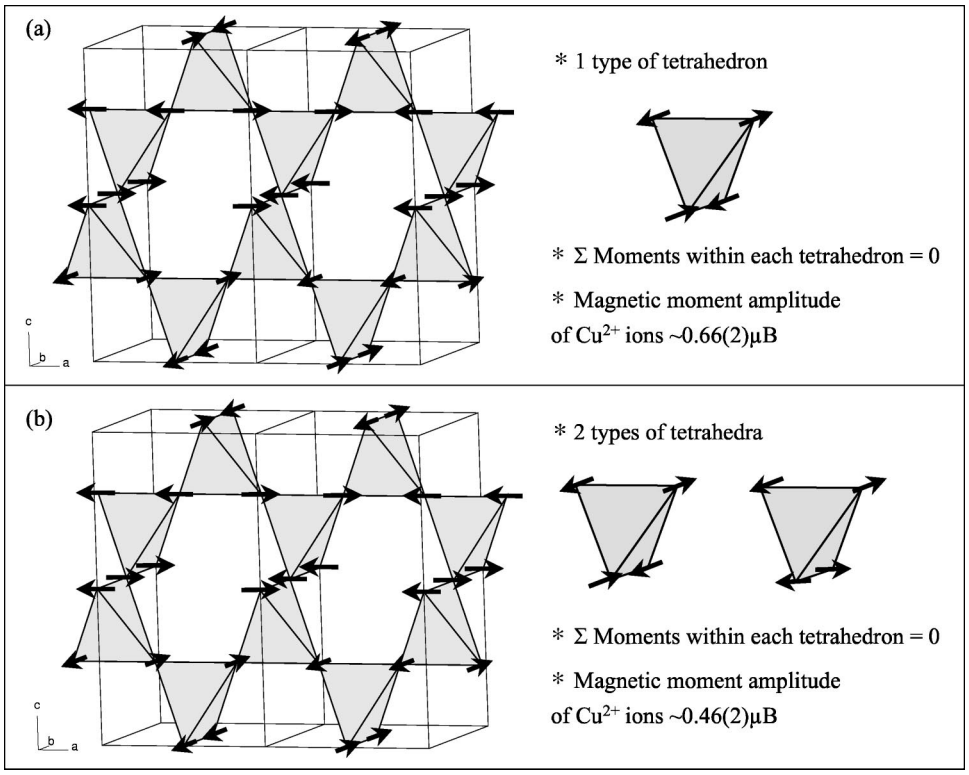

FIG. 4. Collinear (a) and Helical-like model (b) of the magnetic structure of paramelaconite Cu_4O_3.

axis along **c**. The obtained results are summarized in Table I and the two models are illustrated in Figs. 4(a) and 4(b).

In the first model (sinusoidal type) there is only one type of spin configuration satisfying the local condition that the vector sum of spins within each tetrahedron is zero. The amplitude of the magnetic moment carried by the Cu^{+2} ions is $\mu^s_{Cu}=0.66(2)\mu_B$, we obtain a structure similar to that shown in Fig. 4(a).

In the second model (helical type) there are two types of local spin configurations, both satisfying the local condition that the vector sum of spins in each tetrahedron is zero [Fig. 4(b)]. We have to mention that a refinement of the orientation axis of the helix can give a tilt with respect to the **c**-axis improving slightly the reliability index (R factor) of the refinement, but the quality of the data (very weak reflections) does not allow to refine with confidence more free parameters.

The amplitude of the magnetic moment carried by the Cu^{+2} ions for the helical model is, as expected, lower than that of sinusoidal model: $\mu^h_{Cu}=0.46(2)\mu_B$ ($\approx\mu^s_{Cu}/\sqrt{2}$). We can see from Table II that the model 2 (helical-like) gives better reliability indices.

The susceptibility shows a marked anisotropy: the extrapolation of the upturn in the curve to $T=0$, neglecting the extrinsic paramagnetic contribution at low T, indicates that $\chi_c(0)\approx 2\chi_a(0)$. This anisotropy is compatible with both models of the magnetic structure: sinusoidal with magnetic domains and helical, so we cannot use the susceptibility data to support one model against the other. Landau theory states that a *single* irreducible representation is often active in the paramagnetic to magnetic-ordered phase transition, so the helical model is preferred as the actual magnetic structure of paramelaconite because it is well described by the basis functions of the first irreducible representation of the wave vector group (see the Appendix).

DISCUSSION

The observation of magnetic reflections at relatively high temperature was a surprise because a highly frustrated situation was expected. The propagation vector observed in this pyrochlore magnetic lattice is also intriguing. An analysis of the exchange paths considering superexchange interactions, involving up to one oxygen atom bridging the two Cu^{2+} interacting ions, and super-superexchange interactions, involving up to two oxygen atoms interactions, leads to three different isotropic exchange integrals (J_i, $i=1,2,3$), numbered in ascending order of distances between magnetic atoms (see Fig. 5). The single nearest neighbor (NN) exchange integral in a cubic pyrochlore lattice, operating within a tetrahedron, is split in the two integrals J_1 and J_2. These two types of Cu-O-Cu superexchange integrals correspond to intrachain and interchain Cu-O-Cu paths. The interchain Cu-O-Cu paths have a significantly larger Cu-O-Cu angle than those corresponding to the intrachain Cu-O-Cu paths. This difference has a profound effect on the relative strengths of the interchain and intrachain superexchange interactions. Then the interchain NN interaction should be more strongly antiferromagnetic than the intrachain NN interaction. The exchange integral J_3 corresponds to a next-nearest-neighbor (NNN) super-superexchange interaction (Cu-O-O-Cu) along a single CuO_2 chain. This NNN interaction is also intrachain.

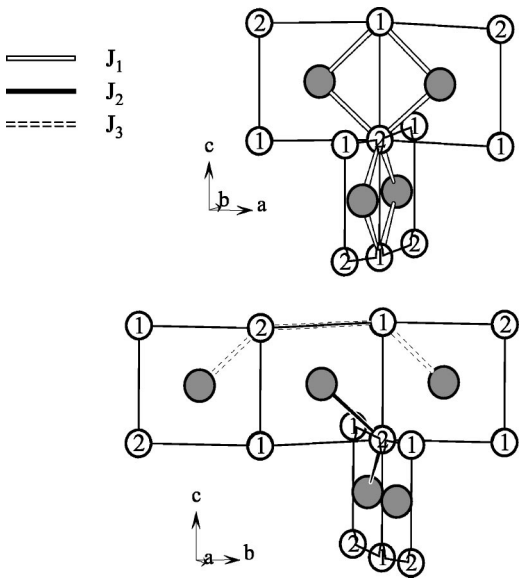

FIG. 5. Representation of the three exchange paths between the copper atoms that have to be considered in Cu_4O_3.

There have been two attempts to determine the value of the exchange interactions in paramelaconite using different methods of electronic structure calculations. Tejada-Rosales *et al.* (TR) (Ref. 18) have calculated the values of the exchange interactions J_1 and J_2 for both paramelaconite and $Ag_2Cu_2O_3$. Whangbo and Koo (WK) (Ref. 19) have determined, using the spin dimer analysis,[20–22] not only the NN interactions but also the NNN exchange integral J_3 (called J_b in their paper). There are important quantitative and qualitative differences between the two calculations concerning the NN interactions. The calculations by WK seem to be more in agreement with the empirical Goudenough-Kanamori-Anderson rules[23–25] for superexchange, however, this does not imply that they use a better method for calculating the exchange integrals. As we will see below none of the values of the exchange integrals provided by electronic structure calculations are sufficient to explain the appearance of the propagation vector $\mathbf{k}=(1/2,1/2,1/2)$. In Table III we give a summary of the exchange interactions relevant to paramelaconite and it isomorphous compound $Ag_2Cu_2O_3$, and the values obtained from electronic structure calculations.

If one adopts a classical mean-field approach for determining the first ordered state it is possible to explore the conditions to be satisfied by the exchange interactions in order to have the propagation vector $\mathbf{k}=(1/2,1/2,1/2)$ the first ordered state that in this particular case coincides with the ground state. The first ordered state is obtained, as a function of $\mathbf{k}$ and the exchange integrals, as the eigenvector corresponding to the maximum eigenvalue of the Fourier transform of the exchange integral matrix (see, for instance, Refs. 26–29):

$$\xi_{ij}(\mathbf{k})=\sum_m J_{ij}(\mathbf{R}_m)\exp\{-2\pi i\mathbf{k}\cdot\mathbf{R}_m\}$$

TABLE III. List of effective exchange interactions considered between copper atoms and geometrical parameters in Cu_4O_3. Values of the exchange parameters of (a) WK and (b) TR.

Interactions	J_1 (Intrachain NN)		J_2 (Interchain NN)	J_3 (Intrachain NNN)
Exchange paths	Cu-O_1-Cu	Cu-O_2-Cu	Cu-O_1-Cu	Cu-O_1-O_2-Cu
Angles	94.5°	99.3°	114.8°	180°
Distances	2.92 Å		3.23 Å	5.84 Å
J (K) values calc.	(a) −17.4		−48.3	(a) −3.9
for Cu_4O_3	(b) −16		−14	
J (K) values calc.	(a) −11.8		−55.4	(a) −3.2
for $Cu_2Ag_2O_3$	(b) −32.5		−33.4	

The indices i, j refer to the magnetic atoms in a primitive cell. $J_{ij}(\mathbf{R}_m)$ is the isotropic exchange interaction between the spins of atoms i and j in units cells separated by the lattice vector $\mathbf{R}_m$. In our case, there are four magnetic atoms of the chemical species per primitive cell, so we have to handle a 4×4 Hermitian matrix.

We have tried to determine the conditions the isotropic exchange interactions farther that next nearest neighbors should satisfy in order to obtain a classical ground state having $\mathbf{k}=(1/2,1/2,1/2)$ as propagation vector. Reimers *et al.*[30] have performed an exhaustive analysis of the perfect pyrochlore lattice within the mean field approximation and there is no region where the propagation vector $\mathbf{k}_C=(0,1,1/2)$ is obtained as first ordered state. In our case the presence of a tetragonal distortion could stabilize somewhere in the J space a region with a propagation vector identical to what we have observed. To do that work we have used the program ENERMAG (Ref. 31) to generate numerical phase diagrams. We have studied in detail the eigenvalues and eigenvectors of the matrix

$$\xi(\mathbf{k},\mathbf{J})=\begin{pmatrix} A & J_2\alpha_y(\alpha_y+\alpha_x\alpha_z) & 2J_1\alpha_x\alpha_z^*\cos\pi y & J_2(1+\alpha_x\alpha_y\alpha_z^*) \\ cc_{12} & B & J_2\alpha_y^*\alpha_z^*(\alpha_x+\alpha_y^*\alpha_z^*) & 2J_1\alpha_y^*\alpha_z^*\cos\pi x \\ cc_{13} & cc_{23} & A & J_2(1+\alpha_x^*\alpha_y\alpha_z) \\ cc_{14} & cc_{24} & cc_{34} & B \end{pmatrix}$$

$$A=2J_3\cos 2\pi y,\quad B=2J_3\cos 2\pi x$$

$$\alpha_b=\exp(\pi ib),\quad \alpha_b^*=\exp(-\pi ib),\quad \text{with } b=x,y \text{ or } z$$

$$cc_{ij}=\text{complex conjugate of element } ij$$

$$\mathbf{k}=(x,y,z)$$

corresponding to the topology of paramelaconite. The program ENERMAG handles the diagonalization of the above matrix. It solves the parametric equation

$$\xi(\mathbf{k},\mathbf{J})\mathbf{v}(\mathbf{k},\mathbf{J})=\lambda(\mathbf{k},\mathbf{J})\mathbf{v}(\mathbf{k},\mathbf{J}),$$

where $\mathbf{J}$ stands for the given set of exchange interactions $\mathbf{J}=\{J_{ij}(\mathbf{R}_m)\}$, and $\mathbf{k}$ is a vector in the asymmetric unit of the BZ. For a given set $\mathbf{J}$, and no degeneracy, the highest eigenvalue $\lambda_{\max}(\mathbf{k}_0,\mathbf{J})$ occurs for a particular $\mathbf{k}_0$, for which the ordering temperature is maximal: $3k_BT_{\max}=\lambda_{\max}(\mathbf{k}_0,\mathbf{J})$. The corresponding eigenvector $\mathbf{v}_{\max}(\mathbf{k}_0,\mathbf{J})$, that may be complex for incommensurate structures, describes the spin configuration of the first ordered state. The program works in fact with the opposite of the exchange matrix, so in our calculations we seek for the minimum eigenvalue. One has to change the sign of the provided eigenvalues to obtain the transition temperature.

We have performed exhaustive calculations using relative values of the exchange interactions in a large volume of the J-space and the results of our calculations indicate that $\mathbf{k}=(1/2,1/2,1/2)=(0,1,1/2)_C$ cannot be obtained as a classical ground state by considering only isotropic exchange interactions. The degree of frustration in the distorted pyrochlore is so high that in the neighborhood of $\mathbf{k}=(1/2,1/2,1/2)$ always exist other propagation vectors with the same classical energy. Of course other well ordered structures, similar to those already described by Reimers,[30] are observed.

As an example of the calculations we present the dispersion relations $E=-\lambda_{\max}(\mathbf{k}_0,\mathbf{J})$ corresponding to some high symmetry directions in the Brillouin zone for the values of the exchange parameters of WK [Fig. 6(a)] and TR [Fig. 6(b)]. As we can see, in the case of neglecting the NNN interaction, we find a strong degeneracy along some reciprocal lattice directions, indicating that, within the classical approach, no order is possible for the values of the exchange integrals calculated by TR. For the values calculated by WK,

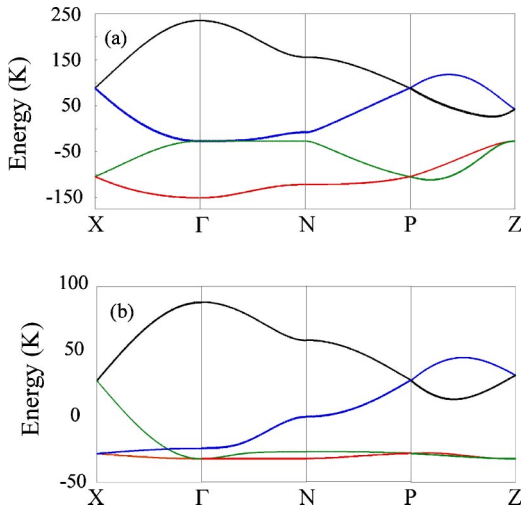

FIG. 6. (Color online) Dispersion relations $E=-\lambda_{max}(\mathbf{k}_0,\mathbf{J})$ corresponding to some high symmetry directions in the Brillouin Zone for the values of the exchange parameters of WK (a) and TR (b). The symmetry points Γ(0,0,0), N (1/2, 0, 1/2), X (1/2, 1/2, 0), Z (1, 1, 1), P (1/2, 1/2, 1/2); are labeled using the notation of Bradley and Cracknell (Ref. 32) but the coordinates are given with respect to the conventional crystallographic reciprocal basis.

the degeneracy is broken and the first ordered state occurs for the propagation vector $\mathbf{k}=(0,0,0)$ giving rise to a collinear structure of the same periodicity as the crystal structure with a sequence $(+,-,+,-)$ for the four spins Cu(2)-1,..., Cu(2)-4 in the primitive cell. As seen in Fig. 6, the value of the energy for point P, which is the observed propagation vector, does not correspond to a minimum in the dispersion relations for none of the sets (WK or TR) of isotropic exchange interactions.

CONCLUSIONS

Paramelaconite orders antiferromagnetically below 40 K with a propagation vector that is, to our knowledge, unprecedented in pyrochlore lattices. Isotropic exchange interactions are unable to give an explanation of the observed propagation vector. This is a surprising result because to first approximation the anisotropy of $S=1/2$ Cu^{2+} ion is quite small. We probably need to invoke either higher order interaction (biquadratic) or anisotropic exchange (symmetric pseudodipolar or antisymmetric Dzyalozinskii-Moriya interactions) in order to explain the observed result. We are presently exploring this issue and the results will be published in a future work.

The amplitude of the magnetic moment carried by Cu^{2+} is small ($\sim 0.46\mu_B$). This small value may indicate a strong covalent character of the Cu-O bonds and the presence of strong fluctuations even at the lowest temperature caused by frustration. A larger crystal is needed to solve some ambiguities concerning the magnetic structure and to perform inelastic magnetic scattering to study the excitations as a function of temperature.

ACKNOWLEDGMENTS

We thank M. Dechamps and J. Jegoudez for help with x-ray orientation and S. Pouget and F. Bourdarot for an attempt on magnetic diffraction under field at the Laue Langevin Institute. We thank C. Lacroix and M. Elhaljal for helpful discussions. We are grateful to P. J. Dunn and D. J. Post from the Smithsonian Institution (Washington) for providing us the paramelaconite crystal.

APPENDIX

The constraints between the components of Fourier coefficients describing the possible magnetic structures can be obtained by symmetry analysis. The Fourier coefficients can be written as linear combinations of the basis functions of irreducible representations (irreps) of the propagation vector group. For details the reader can consult Ref. 16. In Table IV we give the matrices of the two two-dimensional ($d=2$) irreps of the propagation vector group (little group: $I4_1md$). The global magnetic representation Γ_m (Ref. 16) calculated for the Wyckoff position *8d* contains three times the two irreps, so there are six basis functions ($3\times d=6$) for each irrep. In Table IV we also give the basis vectors obtained by the projection operators method using the program BASIREPS.[17] The Fourier coefficients can be obtained using the expression

$$\mathbf{S}_{\mathbf{k}j}=\sum_{n\lambda} C^{\nu}_{n\lambda}\mathbf{S}^{\mathbf{k}\nu}_{n\lambda}(j).$$

The coefficients $C^{\nu}_{n\lambda}$, corresponding to the single irrep Γ_ν, are indexed by n, going from 1 up to the number of repetitions of the irrep Γ_ν within the global magnetic representation, and by λ going from 1 up to $\dim(\Gamma_\nu)$. In our case we have two representations ($\nu=1,2$) of dimension $d=2$ ($\lambda=1,2$) contained three times ($n=1,2,3$) within Γ_m. Calling u, v, w, p, q, r the six coefficients $C^{\nu}_{n\lambda}$ for the first representation in Table IV, we can write for the four Cu atoms the following general expressions of the Fourier coefficients:

$$\mathbf{S}_{\mathbf{k}1}=(u-p,v+q,w+r),\quad \mathbf{S}_{\mathbf{k}2}=(q,p,-r)+i(-v,u,w),$$

$$\mathbf{S}_{\mathbf{k}3}=i(-u-p,-v+q,w-r),$$

$$\mathbf{S}_{\mathbf{k}4}=(v,-u,w)+i(-q,-p,-r).$$

The coefficients may be real or pure imaginary. For the second representation we have the same expressions as above except for a global change of sign for the coefficients of sublattices 2 and 4 (see Table IV). Different values of coefficients determine different magnetic structures belonging to the irreps Γ_ν. If we impose to the free parameters the constraint that the magnetic moment in the different sublattices should have the same modulus, we have to discard all structures with simultaneous non-null parameters u, v, w and p, q, r. We have tested many spin configurations described by the above expressions and the constant moment constraint.

TABLE IV. Irreducible representations of the propagation vector group for $\mathbf{k}=(1/2,1/2,1/2)$ in $I4_1/amd(\mathbf{G}_k=I4_1md)$ and basis functions for axial vectors bound to the Wyckoff site *8d*. The global magnetic representation Γ_m contains three times each irreducible representation: $\Gamma_m=3\Gamma_1\oplus 3\Gamma_2$, so the total number of basis function is six for each representation.

	(x,y,z)	$(-x+1/2,-y,z+1/2)$	$(x,-y,-z)$	$(-x+1/2,y,-z+1/2)$
Γ_1	$\begin{pmatrix}1&0\\0&1\end{pmatrix}$	$\begin{pmatrix}i&0\\0&\bar{i}\end{pmatrix}$	$\begin{pmatrix}0&1\\1&0\end{pmatrix}$	$\begin{pmatrix}0&i\\\bar{i}&0\end{pmatrix}$
Γ_2	$\begin{pmatrix}1&0\\0&1\end{pmatrix}$	$\begin{pmatrix}i&0\\0&\bar{i}\end{pmatrix}$	$\begin{pmatrix}0&1\\1&0\end{pmatrix}$	$\begin{pmatrix}0&i\\\bar{i}&0\end{pmatrix}$
	$(y+3/4,-x+1/4,-z+3/4)$	$(-y+3/4,x+3/4,-z+1/4)$	$(-y+3/4,-x+1/4,z+3/4)$	$(y+3/4,x+3/4,z+1/4)$
Γ_1	$\begin{pmatrix}\bar{1}&0\\0&i\end{pmatrix}$	$\begin{pmatrix}i&0\\0&\bar{1}\end{pmatrix}$	$\begin{pmatrix}0&\bar{1}\\i&0\end{pmatrix}$	$\begin{pmatrix}0&i\\\bar{1}&0\end{pmatrix}$
Γ_2	$\begin{pmatrix}1&0\\0&\bar{i}\end{pmatrix}$	$\begin{pmatrix}\bar{i}&0\\0&1\end{pmatrix}$	$\begin{pmatrix}0&1\\\bar{i}&0\end{pmatrix}$	$\begin{pmatrix}0&\bar{i}\\1&0\end{pmatrix}$
	(x,y,z) Cu(2)-1	$(y+1/4,-x+3/4,-z+5/4)$ Cu(2)-2	$(-x+1/2,-y,z-1/2)$ Cu(2)-3	$(-y+1/4,x+1/4,-z+3/4)$ Cu(2)-4
Γ_1	$(1\ 0\ 0)$	$(0\ i\ 0)$	$(1\ 0\ 0)$	$(0\ \bar{1}\ 0)$
	$(0\ 1\ 0)$	$(\bar{i}\ 0\ 0)$	$(0\ 1\ 0)$	$(1\ 0\ 0)$
	$(0\ 0\ 1)$	$(0\ 0\ i)$	$(0\ 0\ 1)$	$(0\ 0\ 1)$
	$(\bar{1}\ 0\ 0)$	$(0\ 1\ 0)$	$(\bar{1}\ 0\ 0)$	$(0\ \bar{i}\ 0)$
	$(0\ 1\ 0)$	$(1\ 0\ 0)$	$(0\ 1\ 0)$	$(\bar{i}\ 0\ 0)$
	$(0\ 0\ 1)$	$(0\ 0\ \bar{1})$	$(0\ 0\ 1)$	$(0\ 0\ \bar{i})$
Γ_2	$(1\ 0\ 0)$	$(0\ \bar{i}\ 0)$	$(\bar{i}\ 0\ 0)$	$(0\ 1\ 0)$
	$(0\ 1\ 0)$	$(i\ 0\ 0)$	$(0\ \bar{i}\ 0)$	$(\bar{1}\ 0\ 0)$
	$(0\ 0\ 1)$	$(0\ 0\ \bar{i})$	$(0\ 0\ i)$	$(0\ 0\ \bar{1})$
	$(\bar{1}\ 0\ 0)$	$(0\ \bar{1}\ 0)$	$(\bar{i}\ 0\ 0)$	$(0\ i\ 0)$
	$(0\ 1\ 0)$	$(\bar{1}\ 0\ 0)$	$(0\ i\ 0)$	$(i\ 0\ 0)$
	$(0\ 0\ 1)$	$(0\ 0\ 1)$	$(0\ 0\ \bar{i})$	$(0\ 0\ i)$

The helical structure described in the text corresponds to the Fourier coefficients with $w=p=q=r=0$, and $u=1/2\mu^h_{\mathrm{Cu}}$, $v=i/2\mu^h_{\mathrm{Cu}}$, so that

$$\mathbf{S}_{\mathbf{k}1}=(u,v,0)=\frac{\mu^h_{\mathrm{Cu}}}{2}(1,i,0),$$

$$\mathbf{S}_{\mathbf{k}2}=i(-v,u,0)=\frac{\mu^h_{\mathrm{Cu}}}{2}(1,i,0),$$

$$\mathbf{S}_{\mathbf{k}3}=i(-u,-v,0)=\frac{\mu^h_{\mathrm{Cu}}}{2}(1,i,0)e^{-i(\pi/2)},$$

$$\mathbf{S}_{\mathbf{k}4}=(v,-u,0)=\frac{\mu^h_{\mathrm{Cu}}}{2}(1,i,0)e^{i(\pi/2)}.$$

This is a single parameter magnetic structure that provides a good agreement with the experimental data.

The sinusoidal structure described in the main text corresponds to a mixture of the two irreducible representations using as coefficients $w=p=q=r=0$, $w'=p'=q'=r'=0$ and $u=1/4\mu^s_{\mathrm{Cu}}$, $v=i/4\mu^s_{\mathrm{Cu}}$, $u'=1/4\mu^s_{\mathrm{Cu}}$, $v'=-i/4\mu^s_{\mathrm{Cu}}$. The primed coefficients correspond to the second representation. The sum of the Fourier coefficients gives rise to the following result:

$$\mathbf{S}_{\mathbf{k}1}=\frac{\mu^s_{\mathrm{Cu}}}{2}(1,0,0),\quad \mathbf{S}_{\mathbf{k}2}=\frac{\mu^s_{\mathrm{Cu}}}{2}(1,0,0),$$

$$\mathbf{S}_{\mathbf{k}3}=\frac{\mu^s_{\mathrm{Cu}}}{2}(1,0,0)e^{-i(\pi/2)},\quad \mathbf{S}_{\mathbf{k}4}=\frac{\mu^s_{\mathrm{Cu}}}{2}(1,0,0)e^{i(\pi/2)}.$$

This is also a single parameter *collinear* structure that gives a poorer agreement with the experimental data than the helical structure.

[1] J. E. Greedan, J. Mater. Chem. **11**, 37 (2001), and references therein.
[2] R. Moessner, cond-mat/0010301 (unpublished), and references therein.
[3] J. Villain, Z. Phys. **33**, 31 (1979).
[4] G. Ferey, R. de Pape, M. Leblanc, and J. Pannetier, Rev. Chim. Miner. **23**, 474 (1986).
[5] M. O'Keefe and J. O. Bovin, Am. Mineral. **63**, 180 (1978).
[6] Smithsonian Institution, National Museum of Natural History, Ref. 138844 from Bisbee Arizona.
[7] J. F. Pierson, A. Thobor-Keck, and A. Billard, Appl. Surf. Sci. **210**, 359 (2003).
[8] P. E. D. Morgan, D. E. Partin, B. L. Chamberland, and M. O'Kee.e, J. Solid State Chem. **121**, 33 (1996).
[9] J. Rodríguez-Carvajal, Physica B **192**, 55 (1993), URL http:/ www-llb.cea.fr/fullweb/powder.htm
[10] A. Abragam and B. Bleaney, *Electron Paramagnetic Resonance of Transition Ions* (Oxford University Press, Oxford, 1970).
[11] M. P. Gómez-Romero and E. M. Tejada-Rosales, Angew. Chem. Int. Ed. **38**, 524 (1986); Angew. Chem. **11**, 544 (1986).
[12] K. Adelsberger, J. Curda, S. Vensky, and M. Jansen, J. Solid State Chem. **158**, 82 (2001).
[13] E. M. Tejada-Rosales, J. Rodríguez-Carvajal, M. R. Palacín, and P. Gómez-Romero, Mater. Sci. Forum **378-381**, 606 (2001).
[14] L. Pinsard *et al.* (unpublished).
[15] S. Asbrink and L. J. Norrby, Acta Crystallogr., Sect. B: Struct. Crystallogr. Cryst. Chem. **26**, 8 (1970).
[16] Y. A. Izyumov, V. E. Naish, and R. P. Ozerov, *Neutron Diffraction of Magnetic Materials* (Consultants Bureau, Plenum, New York, 1991).
[17] J. Rodríguez-Carvajal, BASIREPS: a program for calculating irreducible representations of space groups and basis functions for axial and polar vector properties, URL ftp://ftp.cea.fr/pub/llb/divers/BasIreps
[18] E. Tejada-Rosales, J. Rodríguez-Carvajal, N. Casañ-Pastor, P. Alemany, E. Ruiz, M. S. El-Fallah, S. Alvarez, and P. Gómez-Romero, Inorg. Chem. **41**, 6604 (2002).
[19] M. H. Whangbo and H. J. Koo, Inorg. Chem. **41**, 3570 (2002).
[20] F. Illas, I. Moreira, D. de Graaf, and V. Barone, Theor. Chem. Acc. **104**, 265 (2000), and the references therein.
[21] L. Noodleman, J. Chem. Phys. **74**, 5737 (1981).
[22] D. Dai and M. H. Whangbo, J. Chem. Phys. **114**, 2887 (2001).
[23] J. B. Goodenough, *Magnetism and the Chemical Bond* (Interscience Publishers, New York, 1963).
[24] J. Kanamori, J. Appl. Phys. **31**, 14S (1960).
[25] P. W. Anderson, *Magnetism A Treatise on Modern Theory and Materials* (Academic Press, New York, 1963), Vol. I.
[26] M. J. Freiser, Phys. Rev. **123**, 2003 (1961).
[27] A. Yoshimori, J. Phys. Soc. Jpn. **14**, 807 (1959).
[28] D. H. Lyons and T. Kaplan, Phys. Rev. **120**, 1580 (1960).
[29] J. Villain, J. Phys. Chem. Solids **11**, 303 (1959).
[30] J. N. Reimers, A. J. Berlinsky, and A. C. Shi, Phys. Rev. B **43**, 865 (1991).
[31] J. Rodríguez-Carvajal (unpublished). The program ENERMAG is shortly described in N. El Khayati, R. Cherkaoui El Moursli, J. Rodríguez-Carvajal, G. André, N. Blanchard, F. Bourée, G. Collin, and T. Roisnel, Eur. Phys. J. B **22**, 4 (2001); G. Rousse, J. Rodríguez-Carvajal, C. Wurm, and C. Masquelier, Solid State Sci. **4**, 973 (2002).
[32] C. J. Bradley and A. P. Cracknell, *The Mathematical Theory of Symmetry in Solids* (Clarendon Press, Oxford, 1972).